Showcasing research from Professor Pema-Tenzin Puno *et al.,* State Key Laboratory of Phytochemistry and Plant Resources in West China, Kunming Institute of Botany, Chinese Academy of Sciences, Yunnan, China.

Discovery and bioinspired total syntheses of unprecedented sesquiterpenoid dimers unveiled bifurcating [4 + 2] cycloaddition and target differentiation of enantiomers

An unprecedented class of cadinane sesquiterpene [4 + 2] dimers were isolated from *Schisandra henryi*. The divergent total syntheses of these natural dimers and their enantiomers were concisely accomplished in eight linear steps using a protection-free approach. Mechanistic studies illustrated the origin of selectivity in the key [4 + 2] cycloaddition as well as the inhibition of reaction pathway bifurcation *via* desymmetrization. The chemical proteomics results showed that a pair of enantiomers shared common targets and had unique targets.

As featured in:
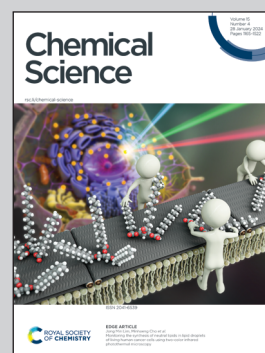
See Xiao-Song Xue, Pema-Tenzin Puno *et al., Chem. Sci.,* 2024, **15**, 1260.

ROYAL SOCIETY
OF **CHEMISTRY**

rsc.li/chemical-science

ROYAL SOCIETY OF CHEMISTRY

Check for updates

Discovery and bioinspired total syntheses of unprecedented sesquiterpenoid dimers unveiled bifurcating [4 + 2] cycloaddition and target differentiation of enantiomers†

Tao-Bin He,‡[a] Bing-Chao Yan, ‡[a] Yuan-Fei Zhou,‡[c] Yue-Qian Sang,‡[b] Xiao-Nian Li,[a] Han-Dong Sun,[a] Chu Wang,[c] Xiao-Song Xue [*b] and Pema-Tenzin Puno [*a]

[4 + 2] cycloaddition has led to diverse polycyclic chiral architectures, serving as novel sources for organic synthesis and biological exploration. Here, an unprecedented class of cadinane sesquiterpene [4 + 2] dimers, henryinins A–E (**1–5**), with a unique 6/6/6/6/6-fused pentacyclic system, were isolated from *Schisandra henryi*. The divergent total syntheses of compounds **1–5** and their enantiomers (**6–10**) were concisely accomplished in eight linear steps using a protection-free approach. Mechanistic studies illustrated the origin of selectivity in the key [4 + 2] cycloaddition as well as the inhibition of reaction pathway bifurcation *via* desymmetrization. The chemical proteomics results showed that a pair of enantiomers shared common targets (PRDX5 C100 and BLMH C73) and had unique targets (USP45 C588 for **4** and COG7 C419 for **9**). This work provides experimental evidence for the discovery of unprecedented cadinane dimers from selective Diels–Alder reaction and a powerful strategy to explore the biological properties of natural products.

Introduction

Natural products arising from [4 + 2] cycloaddition account for a large number of substances in nature, with varying degrees of structural complexity and pharmacological activities.[1–3] The inherent chiral states of polycyclic natural products produced from selective cycloadditions exert diverse biological effects. Given the important relationship between stereochemistry and biological activity, the syntheses of natural products and their enantiomers are expected to increase the potential of screening new frameworks for drug discovery.[4] As one of the most powerful and widely used transformations for carbon–carbon

bond formation, Diels–Alder reactions enable the expedient syntheses of structurally diverse natural products.[5–7] Sesquiterpene dimers, which are naturally occurring metabolites having 30 skeleton carbons, originate biogenetically from two identical or different sesquiterpenoid units.[8] Many bioactive dimeric sesquiterpenoids, particularly guaiane and lindenane dimers, are formed *via* key Diels–Alder reactions (gochnatiolide,[9,10] artemisianin A,[11] schizukaol A,[12–14] and japonicone A[15] in Fig. 1A). The total syntheses of these dimeric sesquiterpenoids remain a great challenge. Furthermore, it is still unclear how the selectivity of cycloaddition is achieved during the formation of these natural enantiomeric dimers.

Cadinane sesquiterpene dimers represent a unique class of sesquiterpene dimers with a wide array of biological activities, including antitumor, anti-inflammation, and anti-HIV properties.[8] Herein, a new class of cadinane sesquiterpene [4 + 2] dimers, henryinins A–E (**1–5**) featuring a unique 6/6/6/6/6-fused pentacyclic skeleton, were isolated from the stems and leaves of *Schisandra henryi* (Fig. 1B). They possess complex stereogenic centers (ten, seven, nine, nine, and ten chiral carbons for **1–5**, respectively) as single enantiomers, demonstrating the peri-, regio-, and stereo-selective features of their biogenetic pathways.

Both enantiomers can be found in the majority of natural products. Additionally, they may exhibit markedly distinct biological and pharmacological behavior in chiral living systems

[a]State Key Laboratory of Phytochemistry and Plant Resources in West China, Kunming Institute of Botany, Chinese Academy of Sciences, Yunnan Key Laboratory of Natural Medicinal Chemistry, Kunming 650201, China. E-mail: punopematenzin@mail.kib.ac.cn

[b]Key Laboratory of Organofluorine Chemistry, Shanghai Institute of Organic Chemistry, University of Chinese Academy of Sciences, Chinese Academy of Sciences, Shanghai200032, China. E-mail: xuexs@sioc.ac.cn

[c]Synthetic and Functional Biomolecules Center, Beijing National Laboratory for Molecular Sciences, Key Laboratory of Bioorganic Chemistry and Molecular Engineering of Ministry of Education, College of Chemistry and Molecular Engineering, Peking University, Beijing 100871, China
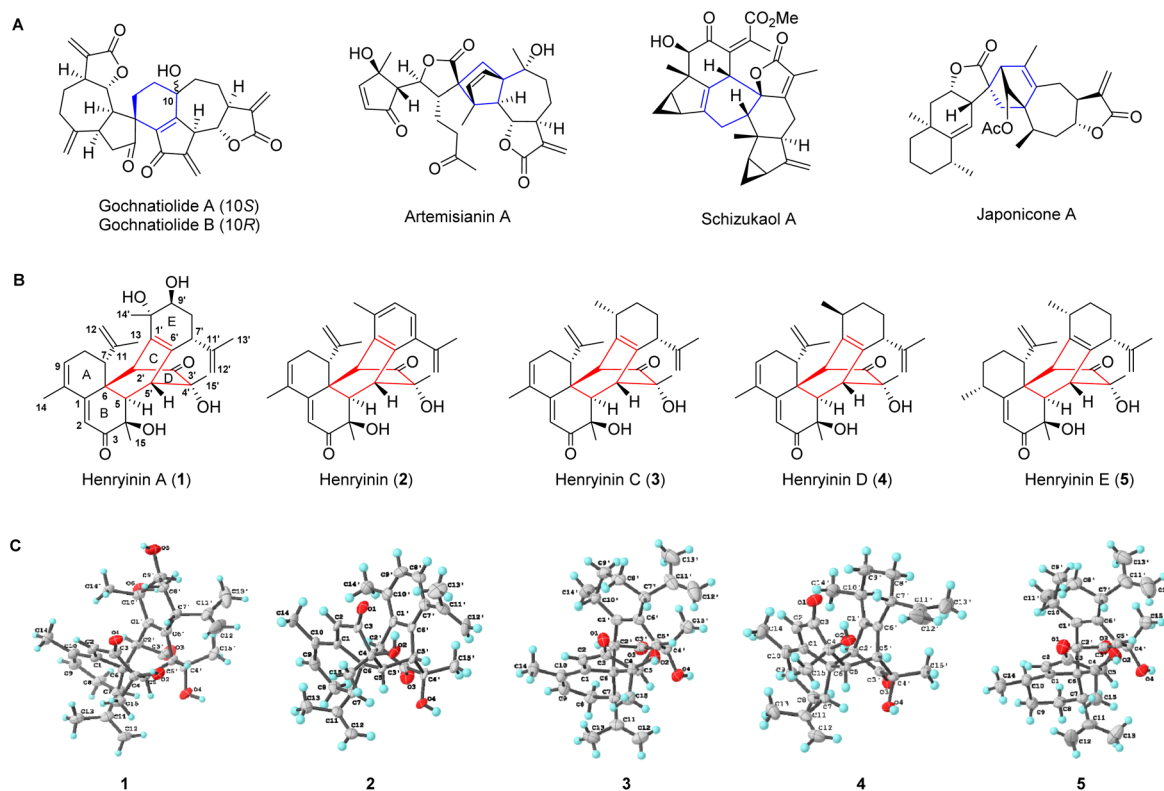
Fig. 1 The structure of dimeric sesquiterpenoids. (A) Selected examples of dimeric sesquiterpenoids. (B and C) Chemical and X-ray structures of henryinins A–E (1–5) bearing complex stereogenic centers (ten, seven, nine, nine, and ten chiral carbons for 1–5, respectively).

because of their different spatial orientations.[16,17] Thus, to investigate the biological activities and provide evidence for the biogenetic pathways of these isolated dimers, the bioinspired and protection-group-free total syntheses of 1–5 and their enantiomers (6–10) were achieved in eight linear steps. The steps mainly included oxidative aromatization via Saegusa–Ito oxidation, oxidative dearomatization, and bifurcating Diels–Alder reactions with high peri-, regio-, and stereo-selectivity. Computational modelling demonstrated the origin of selectivity and the modulation of ambimodal cycloadditions. Given that the enantiomers could bind to different targets, their potential targets were detected using chemical proteomics. The results showed that a pair of enantiomers could share common targets (PRDX5 C100 and BLMH C73) and have their own unique targets (USP45 C588 for 4 and COG7 C419 for 9), providing a powerful strategy to explore the biological properties of natural products.

Results and discussion

Structural elucidation and plausible biogenetic pathways for 1–5

Henryinin A (1), a colorless crystal, possesses a molecular formula of $C_{30}H_{38}O_6$, as determined using high-resolution electrospray ionization mass spectroscopy (HRESIMS) ([M + K]$^+$ m/z 533.2304, calculated 533.2300), indicating 12 degrees of unsaturation. The carbon-13 (^{13}C) nuclear magnetic resonance (NMR), distortionless enhancement by polarization transfer (DEPT), and heteronuclear single quantum coherence (HSQC) spectra of 1 (Table S1, ESI†) revealed 30 carbon signals attributable to six methyl, four methylene (two olefinic), eight methine (two olefinic and one oxygenated), and 12 quaternary carbon (two carbonyl, three oxygenated and six olefinic) groups. The presence of an α, β, γ, δ-unsaturated ketone was indicated by the deshielded chemical shift of C-1 (δ_C 153.4) and the shielded chemical shifts of C-2 (δ_C 123.2) and C-3 carbonyl (δ_C 203.1) together with olefinic C-9 (δ_C 133.4) and C-10 (δ_C 131.9). The above evidence indicated that 1 might be a sesquiterpene dimer fused with a pentacyclic scaffold.

The planar structure of 1 was assigned using two-dimensional (2D) NMR data (Fig. S1, ESI†). The key ^1H–^1H correlation spectroscopy (COSY) correlations of H-7/H$_2$-8/H-9 and the heteronuclear multiple bond correlation (HMBC) results of H-7 with C-1, C-11, C-12, and C-13, H$_2$-8 with C-6 and C-10, and Me-14 with C-1, C-9, and C-10 suggested the presence of a six-membered ring A substituted with C-10 methyl and C-7 isopropenyl groups. The HMBC correlations from H-2 to C-1, C-4, C-6, and C-10, H-5 to C-3, C-4, and C-7, H$_3$-15 to C-3, C-4, and C-5 suggested that a six-membered ring B was fused with ring A. Similarly, a bicyclo[2,2,2]octane-bridged ring system was established using the HMBC correlations of H-2′ with C-5, C-7, and C-10′, H-5′ with C-1′, C-3′, and C-6′, and H$_3$-15 with C-3′, C-4′ and C-5′, together with the ^1H–^1H COSY correlations of H-5/H-5′. The key ^1H–^1H COSY correlations of H-7′/H$_2$-8′/H-9′ along with the HMBC correlations of H-7′ with C-11′, C-12′, and C-13′; H-14′ with C-9′ and C-10′; H-2′ with C-10′; and H-5′ with C-7′ showed

the presence of a six-membered ring E substituted with C-10′ methyl and C-7′ isopropenyl groups. In rotating frame Overhauser effect spectroscopy (ROESY) (Fig. S1†), the cross-peaks of H-5/Me-15 indicated that H-5 and Me-15 were cofacial and adopted α-orientations. The ROESY correlations of H-2′/H-7 suggested that H-2′ and H-7 were vicinally disposed. Considering the biogenetic pathway involving the intermolecular Diels–Alder reaction, H-7 and H-2′ were deduced to be the opposite orientations of H-5 and H-5′, respectively. Thus, H-7 and H-5′ were tentatively assigned as β-orientations, whereas H-2′ was α-oriented. The orientation of Me-15′ was deduced to be β-oriented based on the ROESY correlations of Me-15′/H-5′.

To confirm the structure of 1, high-quality crystals were obtained *via* recrystallization in methanol. An X-ray diffraction study for 1 was successfully performed using anomalous

scattering of CuKα radiation providing conclusive evidence for its absolute configuration (4R,5R,6R,7R,2′S,4′R,5′R,7′R,9′S,10′S) with a Flack parameter of 0.09(4) (Fig. 1C). Compounds 2–5 were determined to be similar to 1, of which the structural elucidation was detailed in the ESI.† Their structures and absolute configurations were confirmed by single-crystal X-ray diffraction analysis (Fig. 1C).

A plausible biogenetic pathway for 1–5 was proposed (Fig. 2A). Based on the reported hypothesis, the formation of sesquiterpenes was considered to originate from farnesyl pyrophosphate (FPP).[18,19] Therefore, ring-forming reactions involving the ionization and cyclization of FPP are proposed to be the initial step in the formation of these compounds. The cationic intermediate 11 would further be transformed into intermediate 12 *via* quenching of the positive charge and loss of

Fig. 2 Design of the total syntheses of henryinins A–E (1–5). (A) Plausible biogenetic pathways of henryinins A–E. (B) Retrosynthetic analysis of henryinins A–E (1–5) in a divergent and protection-free approach.
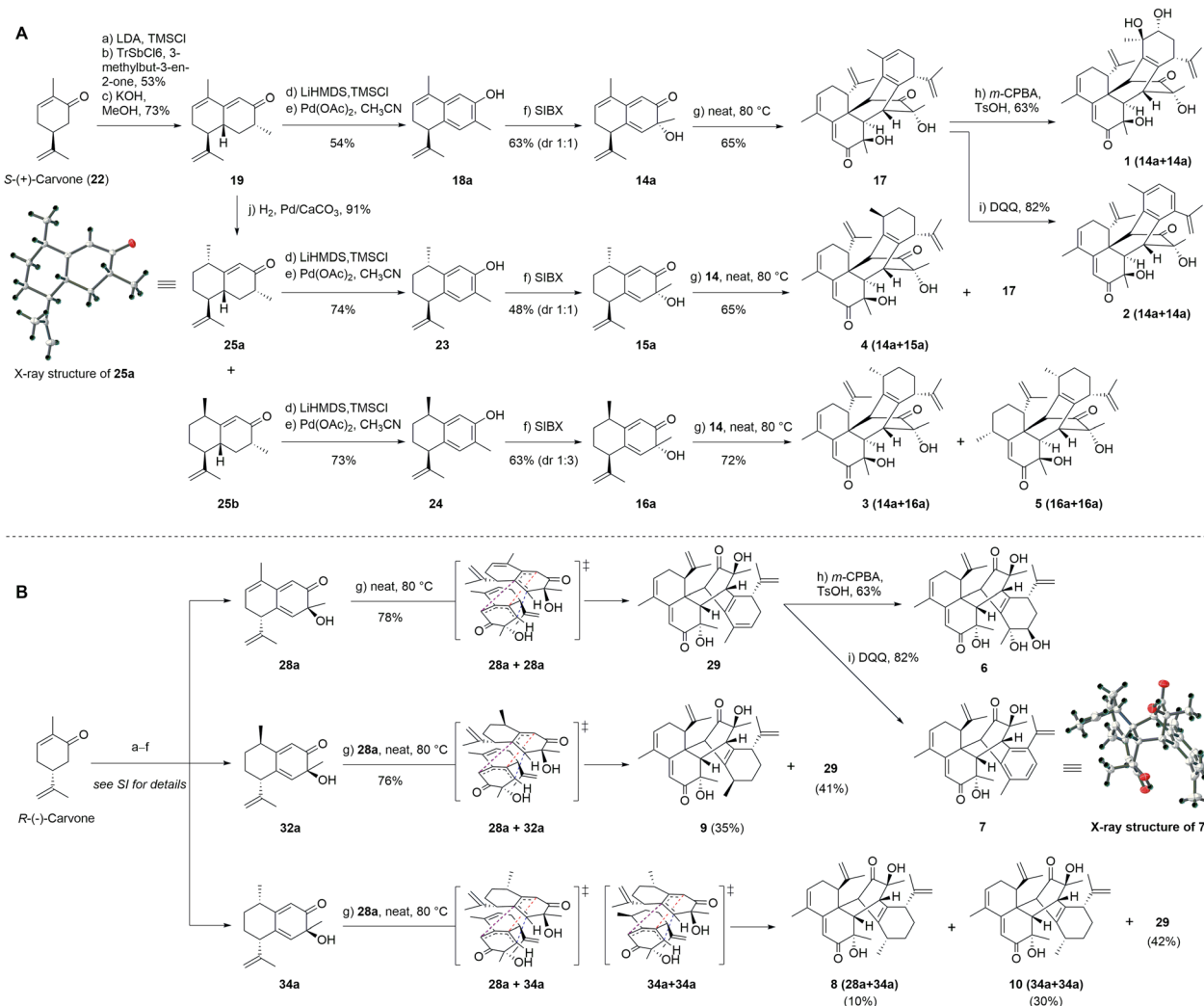
Fig. 3 Bioinspired total syntheses. (A) Henryinins A–E (**1–5**). (B) Enantiomers **6–10** based on the peri-, regio-, and stereo-selectivity of Diels–Alder reaction.

a proton or capture of an external nucleophile such as water or the original pyrophosphate anion. Intermediate **12** would further be transformed into intermediate **13** via oxidation, dehydration, and cyclization. The corresponding precursors (**14a, 15a,** and **16a**) of these compounds could be derived from key intermediate **13** via hydrogenation and oxidation. Finally, the precursors (**14a, 15a,** and **16a**) would be transformed into sesquiterpene dimers with a new carbon skeleton via a key Diels–Alder cycloaddition.

Based on putative biosynthetic pathways, the retrosynthetic analysis of henryinins A–E (**1–5**) is outlined in Fig. 2B. Considering the structural characteristics of the targets, we envisioned that **1** and **2** could be derived from **17** via aromatization[20–23] and dihydroxylation,[24] respectively. Compound **17** could be constructed from intermediate **14a** through an intermolecular Diels–Alder reaction.[25,26] Intermediate **14a** could be generated via dearomatization of **18a,**[27] which could be created by aromatization of **19.**[23,28] Finally, **19** could be prepared from the aldol condensation of **20,** which could be accessed from **21** and

S-(+)-carvone (**22**) through a Michael reaction.[29–31] Using a similar synthetic route, **3–5** could be synthesized from intermediates **23** and **24,** respectively (Fig. 2B).

Bioinspired total syntheses of 1–5 and their enantiomers 6–10

Based on our retrosynthetic analysis, we commenced with the bioinspired and protection group-free syntheses of **1–5** starting from building compound **19,** which was prepared from S-(+)-carvone (**22**) according to a reported procedure (Fig. 3A).[32] The Mukaiyama–Michael reaction of **21** with the kinetic silyl enol ether was accomplished using 5% tritylium hexachloroantimonate as the catalyst to give **20** as a single diastereomer in an overall yield of 53%.[31] The cyclization and methyl isomerization of diketone **20** in the presence of potassium hydroxide (KOH) in methanol at room temperature afforded cadinene sesquiterpenoid **19** in 72% yield.[31] The selective reduction of the γ,δ-double bond of **19** was screened under several conditions, including Pd/C in benzyl alcohol,[33] Pd/C in the presence of hydrogen in hexane,[34] and NaBH$_4$ and

Table 1 Reaction development and the control experiment
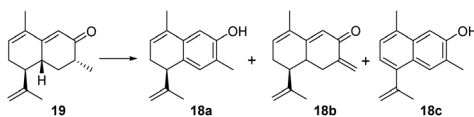
Entry	Conditions	Products	Yield[a] (%)
1	Pd(TFA)$_2$, O$_2$, 2-Me-N-pyridine, *p*-TsOH, DMSO, 80 °C	NR[b]	—
2	LDA, PhSeCl, H$_2$O$_2$	**18b**	67
3	DDQ	NR	—
4	DDQ, TBDMSCl	**18c**	41
5	I$_2$, DMSO, CH$_3$NO$_2$	**18c**	83
6	LiHMDS, TMSCl, Pd(OAc)$_2$, CH$_3$CN	**18a**/**18b** (4 : 1)	54

[a] Isolated yield after chromatography. [b] No reaction.

NiCl$_2$·6H$_2$O in methanol (MeOH) (see Table S6† for details).[35] Finally, the treatment of **19** with palladium on calcium carbonate (CaCO$_3$) produced enone epimers **25a** and **25b** (1 : 3) in an isolated yield of 91%.[34] The absolute configuration of **25a** was confirmed by single-crystal X-ray diffraction analysis.

To achieve the key intermediate phenols **18a**, **23**, and **24**, aromatization reactions were investigated under a variety of conditions.[20,22,23,28,36–39] Initially, palladium(II) trifluoroacetate [Pd(TFA)$_2$] and the corresponding additives [pyridine, and toluenesulfonic acid (TsOH)] were used as catalysts based on the report of Stahl *et al.*[20] However, the aromatization of compound **19** was not observed in our investigation (Table 1, entry 1). Then, we examined the conversion of **19**, **25a**, and **25b** to phenol using lithium diisopropylamide (LDA) and phenylselenyl chloride (PhSeCl) in tetrahydrofuran (THF) followed by oxidation of selenide with 30% hydrogen peroxide (H$_2$O$_2$).[37,38] These conditions were suitable for converting **25a** and **25b**; however, the undesired product **18b** was observed for **19** (Table 1, entry 2). We subjected **19** to 2,3-dichloro-5,6-dicyano-benzoquinone (DDQ); however, the aromatization of **19** did not occur (Table 1, entry 3).[39] When **19** and DDQ were reacted in the presence of 5 mol% *tert*-butyldimethylsilyl chloride (TBSCl) in dioxane at room temperature, the product **18c** was obtained (Table 1, entry 4).[22] However, we could not achieve the desired product *via* the dearomatization of **18c** when we attempted to synthesize the target product **2** by the dearomatization and Diels–Alder reaction of **18c**. Given these challenges, we sequentially sought to explore the dehydrogenative aromatization of **19** *via* metal-free I$_2$ as the catalyst and dimethylsulfoxide (DMSO) as the oxidant.[23] Likewise, undesired product **18c** was generated (Table 1, entry 5). Gratifyingly, inspired by Saegusa–Ito oxidation for enone synthesis,[40] phenols **18a**, **23**, and **24** were afforded *via* oxidative dehydrogenation of **19**, **25a**, and **25b**, respectively (Table 1, entry 6). Although diverse synthetic methods for the dehydrogenation of cyclohexanone have been developed for the preparation of phenols in recent decades, such as metal-catalyzed[20,28,36] or metal-free[23,37,39] oxidative dehydrogenation, to our knowledge, this was the first example of the total synthesis of phenols *via* Saegusa–Ito oxidation. To

improve the efficiency, we further explored the conditions of aromatization using this method (see Table S7† for details).

With ample quantities of phenols **18a**, **23**, and **24** in hand, the key dearomatizing transformation of these phenols was performed using different methods (the detailed optimization procedures are shown in Table S8†). These phenols underwent oxidative dearomatization after treatment with lead(IV) acetate [Pb(OAc)$_4$] to furnish the acetylated product (Table S8,† entry 5). However, the obtained products failed to undergo Diels–Alder cycloaddition and were broken *via* deacetylation with various bases. Finally, the dearomatizing transformation was efficiently accomplished *via* stabilized l$_5$-iodane 2-iodoxybenzoic acid (SIBX)-mediated hydroxylative phenol.[41,42] The oxidation of phenol **18a** with a suspension of SIBX at room temperature produced **14a** and **14b** (1 : 1) in an overall yield of 63%. With **14a** and **14b** in hand, we focused on the formation of a bicyclo[2,2,2] octane-bridged system. Interestingly, we only found the formation of an endo diastereomeric adduct (**17**) of **14a**, which showed the peri-, regio-, and stereo-specific natures of the Diels–Alder reaction. The treatment of key intermediate **17** with *meta*-chloroperoxybenzoic acid (*m*-CPBA) in the presence of *p*-TsOH provided compound **1** in an isolated yield of 67%.[43] The aromatization of **17** proceeded smoothly using DDQ to deliver compound **2**.[37] The treatment of **25a** with a suspension of SIBX at room temperature provided epimers **15a** and **15b** (1 : 1) in 48% yield. Unexpectedly, neither **15a** nor **15b** underwent the Diels–Alder reaction, which may have been a result of the Me-14 configuration.

Fortunately, **15a** and **14a** (1 : 3) were heated at 80 °C to produce compounds **4** and **9**. Compound **25b** underwent dearomatization with a suspension of SIBX at room temperature to generate epimers **16a** and **16b** (1 : 3), resulting from the propensity of spontaneous [4 + 2] cyclodimerizations of **16a**. Compounds **16a** and **14a** were heated at 80 °C to produce compounds **3**, **5**, and **9** (1 : 1 : 2). Thus, the enantioselective preparation of natural products (**1–5**) was effectively accomplished based on the chiral starting material.

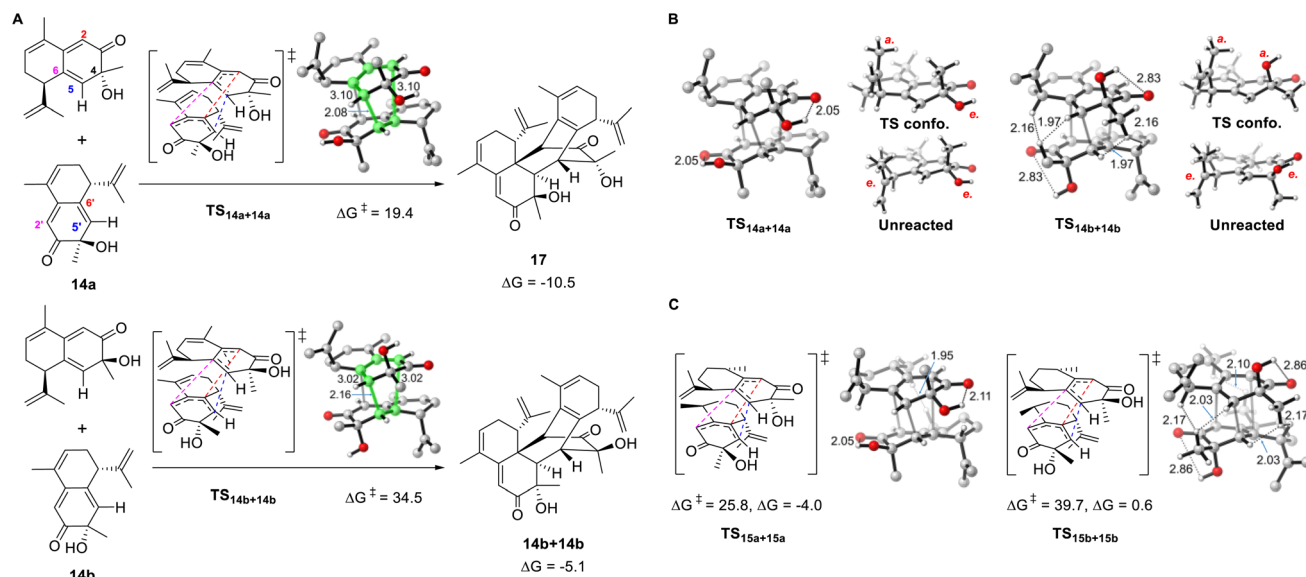In recent years, many enantiomeric natural products have been discovered with distinct biological activities.[44]

Fig. 4 Computational results. (A) Free energy barriers and reaction energies (kcal mol^{-1}) for the homo-dimerization reaction of **14a** and **14b**. (B) Comparison between **TS$_{14a+14a}$** and **TS$_{14b+14b}$** illustrates the origin of stereoselectivity. (C) Homo-dimerization reaction of **15a** and **15b**.

Furthermore, the high level of regioselectivity and peri-selectivity of the Diels–Alder reaction has also been reported recently.[45] To further explore whether the isopropenyl group located at C-7 affected the peri-, regio-, and stereo-selectivity of the Diels–Alder reaction of our intermediates and the biological activities of enantiomeric natural products, we performed the total syntheses of their enantiomers using *R*-(−)-carvone as the starting material. As expected, the total syntheses of enantiomers of natural products (**6–10**) was effectively completed and the Diels–Alder reaction also demonstrated peri-, regio-, and stereo-selectivity (Fig. 3B). The fine synthetic route is outlined in Scheme S1 (ESI†).

Computational studies on the reactivity and origin of selectivity

Density functional theory calculations were conducted to explore the influence of structural differences on the reactivity and selectivity of the dimerization reaction. We chose **14a** and its stereoisomer **14b** for the initial computations. The homo-dimerization of **14a** is both thermodynamically and kinetically favored over that of **14b** (Fig. 4A). The transition state of **14a** (**TS$_{14a+14a}$**) is more stable than that of **TS$_{14b+14b}$** (**14b**) by 15.1 kcal mol^{-1}, which was consistent with the absence of the cycloaddition product for **14b** in the experiments. Moreover, the formation of **17** is more exergonic (by 10.5 kcal mol^{-1}) and is favored over the dimerization product of **14b** (by 5.4 kcal mol^{-1}). The two distorted reactants in **TS$_{14a+14a}$** form a double-layer shape staggered in C$_2$ symmetry, as the dihedral C6–C5–C5′–C6′ angle is 56.1°. **TS$_{14a+14a}$** is an ambimodal transition state that led to two identical adducts, in which the formed C5–C5′ bond is shared, and the competing C6–C2′ or C2–C6′ bond formation afford two equivalent products denoted as [2 + 4] or [4 + 2], respectively.[46–48] Because of the shorter C5–C5′ and longer C6–C2′ or C2–C6′ distances, **TS$_{14a+14a}$** is concerted but

asynchronous.[49] The significant free energy difference of 15.1 kcal mol^{-1} between **TS$_{14a+14a}$** and **TS$_{14b+14b}$** is merely caused by the inversion of the C4 configuration. As shown in Fig. 4B, a glimpse of the **TS$_{14b+14b}$** structure may readily lead to the conclusion that this energy difference is caused by the steric repulsion between the equatorial methyl groups attached to C4 and the neighboring C–H bonds of the other reactant. However, substituting the Me group with H in both **TS$_{14a+14a}$** and **TS$_{14b+14b}$** to release the steric repulsion of Me only decreased the free energy difference to 10.9 kcal mol^{-1} (Fig. S11A†), illustrating this steric effect is not the major reason for the energy difference.

Distortion/interaction analysis was then conducted for the transition states and the derived intrinsic reaction coordinates.[50] Plotting the energies against the length of the forming bond, we noticed that the distortion energies of **14a** and **14b** maintain a constant difference of ∼10 kcal mol^{-1}, and the interaction energy difference was approximately 5 kcal mol^{-1} (Fig. S12†). To maximize the deserved interactions in the transition state, both reactants change conformation as the OH/Me group leaves the equatorial for the axial position of **14b/14a**, respectively. The intramolecular hydrogen bond between OH and C=O in **14a** is kept in **TS$_{14a+14a}$**, but disappeared in **TS$_{14b+14b}$**, implying that its absence caused the high distortion energy of **TS$_{14b+14b}$**. Indeed, if OH is substituted by H, the energy difference of the corresponding transition states decreases to 3.3 kcal mol^{-1} (Fig. S11B†). Therefore, the strong preference for **TS$_{14a+14a}$** over **TS$_{14b+14b}$** is ascribed to the destruction of intramolecular hydrogen bonds and the steric repulsion caused by the Me group in **TS$_{14b+14b}$**, with the former playing a major role. Notably, this origin of stereoselectivity not only reflects the effect of the C4 configuration, but is also suitable for **28b** with an inverted C7 configuration because the corresponding transition state is the mirror image of **TS$_{14b+14b}$**.

In addition to the aforementioned pericyclic reaction of **14a** to produce **17**, the pathways leading to other stereoisomers and regiomers were calculated to be inaccessible (Fig. S13 and S14†), as the energy barriers are >36.0 kcal mol^{-1}. Both intra- and inter-molecular steric repulsions were observed in these transition states. Similar to the unmodified **14a** and **14b**, the homodimerization of **16a** is both thermodynamically and kinetically favored over that of **16b** (Fig. S15†). Unlike **14a**, the homodimerization product of **15a** was not observed in the experiments. Correspondingly, the reaction barrier was calculated to be 25.8 kcal mol^{-1}, in which steric repulsion exists between the Me groups at C10 and C10' (Fig. 4C and S16†).

The cross-dimerization between **14a** and **16a** demonstrated that subtle structural modifications could inhibit the reaction pathway bifurcation and produce a single product. In theory, both **14a** and **16a** could act as dienophiles to react with the other reactant; however, only the former adduct **3** was observed. Accordingly, our computation located **TS$_{14a+16a}$** for the former reaction pathway; however, attempts to find the transition state for the latter reaction failed and led to **TS$_{14a+16a}$**. The merged structure indicates that **TS$_{14a+16a}$** is ambimodal as well (Fig. 5). Compared with the equivalent C6–C2' or C2–C6' distance of 3.10 Å in **TS$_{14a+14a}$**, the larger steric hindrance of the saturated C9–C10 of **16a** than that of the C=C of **14a** elongates the C6–C2' distance to 3.40 Å and increases the dihedral C6–C5–C5'–C6' to 62.6°. Concomitantly, the C2–C6' distance decreases to 2.96 Å because of the seesaw motion of **16a**. Weaker/stronger secondary orbital interactions between C6–C2' and C2–C6' suggest a lower/higher yield of the corresponding product.[51] According to Houk–Yang's empirical equation,[51] the distribution of **3/16a+14a** was predicted to be 64 : 1. A quasi-classical direct molecular dynamics simulation was conducted; however, none of the trajectories initiated from **TS$_{14a+16a}$** terminates at **16a+14a** (Fig. S17†).[52] Moreover, the Cope rearrangement of **3** to produce **16a+14a** has an inaccessible energy barrier of 31.2 kcal mol^{-1}, thus rationalizing the absence of the adduct with **16a** as a dienophile. These results illustrate that the steric hindrance created by structural modification breaks the C$_2$ symmetry and inhibits reaction pathway bifurcation.[51,53–56]

Fig. 5 Reaction pathway bifurcation and the ambimodal TS$_{14a+16a}$ of the cross-dimerization reaction between **14a** and **16a**.

Although the homodimerization of **15a** is accessible, its transformation was enabled by cross-dimerization with **14a**, which has a barrier of 22.5 kcal mol^{-1} via **TS$_{14a+15a}$** (Fig. S18†). The energy difference of 3.3 kcal mol^{-1} between **TS$_{15a+15a}$** and **TS$_{14a+15a}$** excludes the homodimerization reaction. Moreover, the computed barriers increase in an order from **TS$_{14a+14a}$** to **TS$_{15a+15a}$**, which reproduced the experimental product distribution. Similar to **14a** and **16a**, the cross-dimerization of **14a** and **15a** failed to generate the adduct with **15a** as a dienophile because bifurcation is inhibited (Fig. S19†).

Chemoproteomic profiling of a pair of enantiomers by the competitive rdTOP-ABPP method

We reasoned that the $\alpha,\beta,\gamma,\delta$-unsaturated ketone groups of compounds **1–10** would capture thiol groups and form C–S covalent bonds with the cysteine residues of the target proteins. Therefore, we could explore whether there are active cysteines in the proteome that can covalently bind to the compounds, thereby identifying the potential target of the compound. The isotopic tandem orthogonal proteolysis-activity-based protein profiling (isoTOP-ABPP) method, an advanced derivative of Activity-Based Protein Profiling (ABPP),[57] employs a cysteine-reactive iodoacetamide probe functionalized with a bio-orthogonal alkyne handle [iodoacetamide (IA)-alkyne] and a pair of isotopically encoded cleavable azide-biotin tags to enable quantification of intrinsic cysteine reactivity.[58] Additionally, it can be used for mapping druggable hotspots targeted by covalently acting metabolites.[59] Recently, the rdTOP-ABPP method was introduced to enhance the pipeline by incorporating reductive dimethylation for triplex quantitation to broadly functional cysteinomes.[60] The above methods were designed to determine if the compounds can covalently bind to cysteines and compete with IA-alkyne. Briefly, the $\alpha,\beta,\gamma,\delta$-unsaturated ketone groups in **1–10** likely reacted with cysteine residues of target proteins because the sulfur atoms of cysteine residues will have strong nucleophilic reactivity, when the sulfhydryl groups are deprotonated. When cysteine residues form covalent bonds with compounds, fewer cysteine residues undergo nucleophilic substitution reactions with IA-alkyne compared with the DMSO group. Subsequent visualization of IA-alkyne using azide-rhodamine will produce less fluorescence. Therefore, we first evaluated whether these compounds could compete with IA-alkyne in cell lysates using in-gel fluorescence. HT1080 cell lysates were treated with 100 μM compounds **1–10**, labelled with IA-alkyne and then visualized using azide-rhodamine via copper-catalyzed azide–alkyne cycloaddition (CuAAC) (Fig. S19†).

Compounds **3**, **4** and **9** showed weaker fluorescence than the vehicle group (vehicle group was added DMSO as a control), indicating that the three compounds likely have stronger reactivity with cysteine residues than other groups and showed competition with IA-alkyne (Fig. 6A). Given that **4** and **9** are a pair of enantiomers, the two compounds were also studied. The fluorescence of **4** and **9** decreased with increasing compound concentrations, suggesting that competition against IA-alkyne was concentration-dependent (Fig. 6B). Although
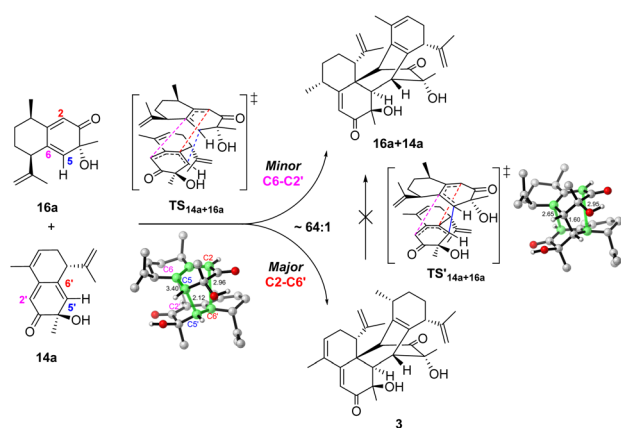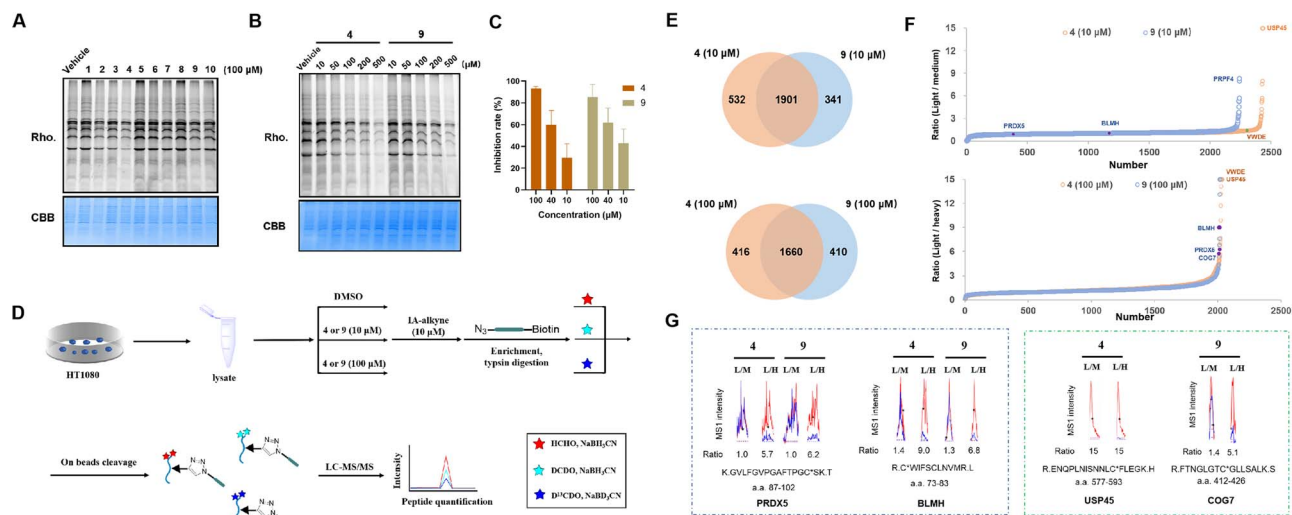
Fig. 6 Chemical proteomic profiling by competitive rdTOP-ABPP. (A) The HT1080 cell lysates were incubated with compounds **1–10** and visualized by in-gel fluorescence; (B) the fluorescence decreased as the concentrations of **4** and **9** increased; (C) cytotoxic experiments demonstrated that **4** showed similar inhibition rates to **9** at three concentrations; (D) the scheme of quantitative profiling of reactive cysteines by rdTOP-ABPP; (E) a Venn diagram showing the number of re-active cysteine peptides quantified from **4** and **9** at a 10 or 100 μM level; (F) the rdTOP-ABPP ratios for each cysteine site quantified at a 10 or 100 μM level; (G) representative MS1 profiles for peptides that show common targets (PRDX5 and BLMH) for **4** and **9**, and unique targets for **4** (USP45) and **9** (COG7).

cytotoxic experiments on HT1080 cells demonstrated that **4** showed similar inhibition rates to **9** at three concentrations (Fig. 6C), whether the targets of the natural product (**4**) differed from its enantiomer (**9**) remains unclear. Therefore, we performed comprehensive profiling of **4** and **9** in HT1080 cell lysates using rdTOP-ABPP. The HT1080 whole cell lysates were first treated with DMSO, **4** or **9** (10 μM and 100 μM), and then labeled separately with the IA-alkyne probe. After enrichment with streptavidin and on-bead trypsin digestion, the probe-adducted peptides from DMSO, **4** or **9** (10 μM and 100 μM), were isotopically labeled with light, medium, and heavy dimethylation reagents, respectively (Fig. 6D). The samples were subjected to acid cleavage, and the released peptides were analyzed using liquid chromatography with tandem mass spectrometry (LC-MS/MS) and quantified using CIMAGE 2.0 software.[61] We performed three biological replicates for both experiments, and the peptides quantified in at least two out of the three replicates were considered for further analysis. The light/medium [DMSO/**4** or **9** (10 μM)] ratio and the light/heavy [DMSO/**4** or **9** (100 μM)] ratio reflected the competitiveness of the given compounds with IA-alkyne (Fig. 6D and S20†). Finally, 1901 targets were quantified under the 10 μM compound treatment, and 1660 targets were quantified under the 100 μM compound treatment (Fig. 6E). Among the candidate targets (Fig. 6F), we chose these targets for two reasons. One is that the spectrum has a high degree of confidence, requiring a good fit (R^2) value between the light/medium/heavy groups and stable performance across three replicates. The other is its concentration-dependent features, meaning that the ratio of the high-concentration group (100 μM) was higher than that of the low-concentration group (10 μM). In the candidates, PRDX5 C100 and BLMH C73 both met the above criteria in the two

groups and were considered as common targets of compounds **4** and **9** (Fig. 6G, for more see the ESI†). USP45 C588 was detected only in the compound **4** group but not in the compound **9** group and was thought to be a specific target for **4**. The dose–effect relationship of USP45 C588 was not shown at high and low concentrations in the compound **4** group, mainly because the competition reached saturation at low concentrations (the highest ratio value was 15) (Fig. 6G, for more see ESI†). COG7 C419 was detected in both the compound **4** group and compound **9** group. However, COG7 C419 showed a concentration-dependent feature only in the compound **9** group and was considered to be a specific target for **9**.

Data availability

All experimental and characterization data, as well as NMR spectra, are available in the ESI. Crystallographic data for the structures reported in this paper have been deposited at the Cambridge Crystallographic Data Centre "https://www.ccdc.cam.ac.uk/", under the accession numbers CCDC: 2212935, 2212936, 2212937, 2212938, 2212942, 2212943, 2212947, 2212950 for **1–5**, **7**, **25a**, and **30a**, respectively.†

Author contributions

T.-B. H., B.-C. Y., Y.-F. Z., and Y.-Q. S. contributed equally to this work. T.-B. H.: conceptualization, data curation, investigation, writing original draft, and visualization, B.-C. Y.: conceptualization, data curation, visualization, validation, and writing – review & editing, Y.-F. Z.: conceptualization, data curation, investigation, writing original draft, and visualization, Y.-Q. S.: conceptualization, data curation, investigation, writing original

draft, and visualization. X.-N. L.: data curation and investigation, H.-D. S.: supervision, C. W.: supervision, writing – review & editing, conceptualization, and validation, X.-S. X.: supervision, writing – review & editing, conceptualization, and validation, P.-T. P.: supervision, funding acquisition, writing – review & editing, conceptualization, resources, and validation.

Conflicts of interest

The authors declare no competing interests.

Acknowledgements

Notes and references

1 J. Clardy and C. Walsh, Lessons from natural molecules, *Nature*, 2004, **432**, 829–837.

2 H. Oikawa and T. Tokiwano, Enzymatic catalysis of the Diels–Alder reaction in the biosynthesis of natural products, *Nat. Prod. Rep.*, 2004, **21**, 321–352.

3 C. Li, T. Dong, L. Dian, W. Zhang and X. Lei, Biomimetic syntheses and structural elucidation of the apoptosis-inducing sesquiterpenoid trimers: (−)-ainsliatrimers A and B, *Chem. Sci.*, 2013, **4**, 1163–1167.

4 Y. Wang, M. M. Dix, G. Bianco, J. R. Remsberg, H.-Y. Lee, M. Kalocsay, S. P. Gygi, S. Forli, G. Vite, R. M. Lawrence, C. G. Parker and B. F. Cravatt, Expedited mapping of the ligandable proteome using fully functionalized enantiomeric probe pairs, *Nat. Chem.*, 2019, **11**, 1113–1123.

5 R.-B. Wang, S.-G. Ma, C. S. Jamieson, R.-M. Gao, Y.-B. Liu, Y. Li, X.-J. Wang, Y.-H. Li, K. N. Houk, J. Qu and S.-S. Yu, Library construction of stereochemically diverse isomers of spirooliganin: their total synthesis and antiviral activity, *Chem. Sci.*, 2021, **12**, 7003–7011.

6 K.-I. Takao, R. Munakata and K.-I. Tadano, Recent advances in natural product synthesis by using intramolecular Diels−Alder reactions, *Chem. Rev.*, 2005, **105**, 4779–4807.

7 J.-L. Li, S.-L. Zhou, P.-Q. Chen, L. Dong, T.-Y. Liu and Y.-C. Chen, Asymmetric Diels–Alder reaction of β,β-disubstituted enals and chromone-fused dienes: construction of collections with high molecular complexity and skeletal diversity, *Chem. Sci.*, 2012, **3**, 1879–1882.

8 L.-F. Ma, Y.-L. Chen, W.-G. Shan and Z.-J. Zhan, Natural disesquiterpenoids: an update, *Nat. Prod. Rep.*, 2020, **37**, 999–1030.

9 Y. Chen, W. Li, Z. Zeng and Y. Tang, (−)-Gochnatiolide B, synthesized from dehydrocostuslactone, exhibits potent anti-bladder cancer activity in vitro and in vivo, *Sci. Rep.*, 2018, **8**, 8807.

10 C. Li, L. Dian, W. Zhang and X. Lei, Biomimetic syntheses of (−)-gochnatiolides A–C and (−)-ainsliadimer B, *J. Am. Chem. Soc.*, 2012, **134**, 12414–12417.

11 G.-M. Xue, D.-R. Zhu, C. Han, X.-B. Wang, J.-G. Luo and L.-Y. Kong, Artemisianins A–D, new stereoisomers of seco-guaianolide involved heterodimeric [4+2] adducts from Artemisia argyi induce apoptosis via enhancement of endoplasmic reticulum stress, *Bioorg. Chem.*, 2019, **84**, 295–301.

12 B. Du, Z. Huang, X. Wang, T. Chen, G. Shen, S. Fu and B. Liu, A unified strategy toward total syntheses of lindenane sesquiterpenoid [4 + 2] dimers, *Nat. Commun.*, 2019, **10**, 1892.

13 J.-L. Wu, Y.-S. Lu, B. Tang and X.-S. Peng, Total syntheses of shizukaols A and E, *Nat. Commun.*, 2018, **9**, 4040.

14 C. Yuan, B. Du, H. Deng, Y. Man and B. Liu, Total syntheses of sarcandrolide J and shizukaol D: lindenane sesquiterpenoid [4+2] dimers, *Angew. Chem., Int. Ed.*, 2017, **56**, 637–640.

15 J. J. Qin, H. Z. Jin, J. J. Fu, X. J. Hu, Y. Wang, S. K. Yan and W. D. Zhang, Japonicones A–D, bioactive dimeric sesquiterpenes from *Inula japonica thunb*, *Bioorg. Med. Chem. Lett.*, 2009, **19**, 710–713.

16 X. Kang, E. R. Stephens, B. M. Spector-Watts, Z. Li, Y. Liu, L. Liu and Y. Cui, Challenges and opportunities for chiral covalent organic frameworks, *Chem. Sci.*, 2022, **13**, 9811–9832.

17 M. Quack, G. Seyfang and G. Wichmann, Perspectives on parity violation in chiral molecules: theory, spectroscopic experiment and biomolecular homochirality, *Chem. Sci.*, 2022, **13**, 10598–10643.

18 D. E. Cane, Enzymic formation of sesquiterpenes, *Chem. Rev.*, 1990, **90**, 1089–1103.

19 Y. J. Hong and D. J. Tantillo, Consequences of conformational preorganization in sesquiterpene biosynthesis: theoretical studies on the formation of the bisabolene, curcumene, acoradiene, zizaene, cedrene, duprezianene, and sesquithuriferol sesquiterpenes, *J. Am. Chem. Soc.*, 2009, **131**, 7999–8015.

20 D. Pun, T. Diao and S. S. Stahl, Aerobic dehydrogenation of cyclohexanone to phenol catalyzed by $Pd(TFA)_2$/2-dimethylaminopyridine: evidence for the role of Pd nanoparticles, *J. Am. Chem. Soc.*, 2013, **135**, 8213–8221.

21 K. J. Shea, L. D. Burke and R. J. Doedens, A novel synthesis of metacyclophanes. Thermal and DDQ induced aromatization of bridgehead dienes, *J. Am. Chem. Soc.*, 1985, **107**, 5305–5306.

22 K. Chen, C. Liu, L. Deng and G. Xu, A practical Δ^1-dehydrogenation of Δ^4-3-keto-steroids with DDQ in the

presence of TBDMSCl at room temperature, *Steroids*, 2010, **75**, 513–516.

23 Y.-F. Liang, S. Song, L. Ai, X. Li and N. Jiao, A highly efficient metal-free approach to meta- and multiple-substituted phenols via a simple oxidation of cyclohexenones, *Green Chem.*, 2016, **18**, 6462–6467.

24 C. Bonini and G. Righi, A critical outlook and comparison of enantioselective oxidation methodologies of olefins, *Tetrahedron*, 2002, **58**, 4981–5021.

25 A. Sib and T. A. M. Gulder, Stereoselective total synthesis of bisorbicillinoid natural products by enzymatic oxidative dearomatization/dimerization, *Angew. Chem., Int. Ed.*, 2017, **56**, 12888–12891.

26 S. Dong, K. J. Cahill, M.-I. Kang, N. H. Colburn, C. J. Henrich, J. A. Wilson, J. A. Beutler, R. P. Johnson and J. A. Porco Jr, Microwave-based reaction screening: tandem retro-Diels–Alder/Diels–Alder cycloadditions of o-quinol dimers, *J. Org. Chem.*, 2011, **76**, 8944–8954.

27 K. C. Nicolaou, K. B. Simonsen, G. Vassilikogiannakis, P. S. Baran, V. P. Vidali, E. N. Pitsinos and E. A. Couladouros, Biomimetic explorations towards the bisorbicillinoids: total synthesis of bisorbicillinol, bisorbibutenolide, and trichodimerol, *Angew. Chem., Int. Ed.*, 1999, **38**, 3555–3559.

28 I. Y. El-Deeb, M. Tian, T. Funakoshi, R. Matsubara and M. Hayashi, Conversion of cyclohexanones to alkyl aryl ethers by using a Pd/C–ethylene system, *Eur. J. Org Chem.*, 2017, **2017**, 409–413.

29 K.-S. Ngo and G. D. Brown, Synthesis of amorphane and cadinane sesquiterpenes from fabiana imbricata, *Tetrahedron*, 1999, **55**, 15099–15108.

30 J. Beauhaire, P.-H. Ducrot and I. Simon, Synthesis of diaprepal A₂ cadinane analogs; efficient access to polyoxygenated cadinanes, *Synth. Commun.*, 1995, **25**, 3015–3025.

31 A. V. Baranovsky, B. J. M. Jansen, T. M. Meulemans and A. de Groot, Enantioselective synthesis of cadinanes starting from R-(−)- or S-(+)-carvone, *Tetrahedron*, 1998, **54**, 5623–5634.

32 E. F. Landau and E. P. Irany, Preparation of methyl isopropenyl ketone from methyl ethyl ketone and formaldehyde, *J. Org. Chem.*, 1947, **12**, 422–425.

33 R. Vitali, G. Caccia and R. Gardi, Benzyl alcohol as hydrogen donor in selective transfer hydrogenation of unsaturated steroids, *J. Org. Chem.*, 1972, **37**, 3745–3746.

34 P. Kraft, S. Jordi, N. Denizot and I. Felker, On the dienone motif of musks: synthesis and olfactory properties of partially and fully hydrogenated dienone musks, *Eur. J. Org Chem.*, 2014, **2014**, 554–563.

35 J. Liu, J. Wu, J.-H. Fan, X. Yan, G. Mei and C.-C. Li, Asymmetric total synthesis of cyclocitrinol, *J. Am. Chem. Soc.*, 2018, **140**, 5365–5369.

36 J. Zhang, Q. Jiang, D. Yang, X. Zhao, Y. Dong and R. Liu, Reaction-activated palladium catalyst for dehydrogenation of substituted cyclohexanones to phenols and H₂ without oxidants and hydrogen acceptors, *Chem. Sci.*, 2015, **6**, 4674–4680.

37 C. X. Zhang, F. Q. Bi and Y. L. Li, The first total synthesis of ligudentatin A, *Chin. Chem. Lett.*, 2008, **19**, 805–806.

38 M. I. Al-hassan, Conversion of 19-nortestosterone to β-estradiol, *Synth. Commun.*, 1989, **19**, 453–461.

39 J. A. Robl, A new and versatile route for the synthesis of highly substituted benzenoids, *Tetrahedron Lett.*, 1990, **31**, 3421–3424.

40 Y. Ito, T. Hirao and T. Saegusa, Synthesis of α,β-unsaturated carbonyl compounds by palladium(II)-catalyzed dehydrosilylation of silyl enol ethers, *J. Org. Chem.*, 1978, **43**, 1011–1013.

41 N. Lebrasseur, J. Gagnepain, A. Ozanne-Beaudenon, J.-M. Léger and S. Quideau, Efficient access to orthoquinols and their [4 + 2] cyclodimers via SIBX-mediated hydroxylative phenol dearomatization, *J. Org. Chem.*, 2007, **72**, 6280–6283.

42 J. Gagnepain, F. Castet and S. Quideau, Total synthesis of (+)-aquaticol by biomimetic phenol dearomatization: double diastereofacial differentiation in the Diels–Alder dimerization of orthoquinols with a C₂-symmetric transition state, *Angew. Chem., Int. Ed.*, 2007, **46**, 1533–1535.

43 T. W. Bingham, L. W. Hernandez, D. G. Olson, R. L. Svec, P. J. Hergenrother and D. Sarlah, Enantioselective synthesis of isocarbostyril alkaloids and analogs using catalytic dearomative functionalization of benzene, *J. Am. Chem. Soc.*, 2019, **141**, 657–670.

44 Y. Chen, G. B. Craven, R. A. Kamber, A. Cuesta, S. Zhersh, Y. S. Moroz, M. C. Bassik and J. Taunton, Direct mapping of ligandable tyrosines and lysines in cells with chiral sulfonyl fluoride probes, *Nat. Chem.*, 2023, **15**, 1616–1625.

45 M. Ohashi, C. S. Jamieson, Y. Cai, D. Tan, D. Kanayama, M.-C. Tang, S. M. Anthony, J. V. Chari, J. S. Barber, E. Picazo, T. B. Kakule, S. Cao, N. K. Garg, J. Zhou, K. N. Houk and Y. Tang, An enzymatic Alder-ene reaction, *Nature*, 2020, **586**, 64–69.

46 P. Caramella, P. Quadrelli and L. Toma, An unexpected bispericyclic transition structure leading to 4+2 and 2+4 cycloadducts in the endo dimerization of cyclopentadiene, *J. Am. Chem. Soc.*, 2002, **124**, 1130–1131.

47 D. H. Ess, S. E. Wheeler, R. G. Iafe, L. Xu, N. Çelebi-Ölçüm and K. N. Houk, Bifurcations on potential energy surfaces of organic reactions, *Angew. Chem., Int. Ed.*, 2008, **47**, 7592–7601.

48 D. J. Tantillo, Dynamic effects on organic reactivity—Pathways to (and from) discomfort, *J. Phys. Org. Chem.*, 2021, **34**, e4202.

49 Z. Yang, C. S. Jamieson, X.-S. Xue, M. Garcia-Borràs, T. Benton, X. Dong, F. Liu and K. N. Houk, Mechanisms and dynamics of reactions involving entropic intermediates, *Trends Chem.*, 2019, **1**, 22–34.

50 F. M. Bickelhaupt and K. N. Houk, Analyzing reaction rates with the distortion/interaction-activation strain model, *Angew. Chem., Int. Ed.*, 2017, **56**, 10070–10086.

51 S. Chen, P. Yu and K. N. Houk, Ambimodal dipolar/Diels–Alder cycloaddition transition states involving proton transfers, *J. Am. Chem. Soc.*, 2018, **140**, 18124–18131.

52 S. Pratihar, X. Ma, Z. Homayoon, G. L. Barnes and W. L. Hase, Direct chemical dynamics simulations, *J. Am. Chem. Soc.*, 2017, **139**, 3570–3590.

53 H. Yamataka, M. Sato, H. Hasegawa and S. C. Ammal, Dynamic path bifurcation for the Beckmann reaction: observation and implication, *Faraday Discuss.*, 2010, **145**, 327–340.

54 J. B. Thomas, J. R. Waas, M. Harmata and D. A. Singleton, Control elements in dynamically determined selectivity on a bifurcating surface, *J. Am. Chem. Soc.*, 2008, **130**, 14544–14555.

55 R. B. Campos and D. J. Tantillo, Designing reactions with post-transition-state bifurcations: asynchronous nitrene insertions into C–C σ bonds, *Chem*, 2019, **5**, 227–236.

56 S. R. Hare, R. P. Pemberton and D. J. Tantillo, Navigating past a fork in the road: carbocation−π interactions can manipulate dynamic behavior of reactions facing post-transition-state bifurcations, *J. Am. Chem. Soc.*, 2017, **139**, 7485–7493.

57 Y. Liu, M. P. Patricelli and B. F. Cravatt, Activity-based protein profiling: the serine hydrolases, *Proc. Natl. Acad. Sci. U. S. A.*, 1999, **96**, 14694–14699.

58 E. Weerapana, C. Wang, G. M. Simon, F. Richter, S. Khare, M. B. D. Dillon, D. A. Bachovchin, K. Mowen, D. Baker and B. F. Cravatt, Quantitative reactivity profiling predicts functional cysteines in proteomes, *Nature*, 2010, **468**, 790–795.

59 C. Wang, E. Weerapana, M. M. Blewett and B. F. Cravatt, A chemoproteomic platform to quantitatively map targets of lipid-derived electrophiles, *Nat. Methods*, 2014, **11**, 79–85.

60 F. Yang, J. Gao, J. Che, G. Jia and C. Wang, A dimethyl-labeling-based strategy for site-specifically quantitative chemical proteomics, *Anal. Chem.*, 2018, **90**, 9576–9582.

61 J. Gao, Y. Liu, F. Yang, X. Chen, B. F. Cravatt and C. Wang, CIMAGE2.0: an expanded tool for quantitative analysis of activity-based protein profiling (ABPP) Data, *J. Proteome Res.*, 2021, **20**, 4893–4900.